



Short communication

Reliable benchmark material for anatase TiO₂ in Li-ion batteries: On the role of dehydration of commercial TiO₂

Edyta Madej^{a,b}, Fabio La Mantia^b, Bastian Mei^c, Stefan Klink^a, Martin Muhler^c,
Wolfgang Schuhmann^{a,b}, Edgar Ventosa^{a,*}

^aAnalytische Chemie – Elektroanalytik & Sensorik, Ruhr-Universität Bochum, Universitätsstr. 150, 44780 Bochum, Germany

^bCenter for Electrochemical Sciences – CES, Ruhr-Universität Bochum, Universitätsstr. 150, 44780 Bochum, Germany

^cLaboratory of Industrial Chemistry, Ruhr-Universität Bochum, Universitätsstr. 150, 44780 Bochum, Germany

H I G H L I G H T S

- Commercial TiO₂ nanoparticles for Li-ion batteries fails in cyclability.
- Li-ions are entrapped inside TiO₂ upon cycling.
- Annealing in air of commercial TiO₂ leads to remarkable improvement.
- Air-annealed commercial TiO₂ becomes an excellent TiO₂ benchmark material.

A R T I C L E I N F O

Article history:

Received 6 February 2014

Received in revised form

8 April 2014

Accepted 3 May 2014

Available online 14 May 2014

Keywords:

Li-ion battery

Anatase TiO₂

Benchmark material

Cyclability

Dehydration

A B S T R A C T

Commercially available anatase TiO₂ nanoparticles (ca. 15–20 nm particle size) were investigated as negative electrode material for Li-ion batteries. Despite the high initial specific charge of 200 mAh g^{−1} at 0.5C, the pristine commercial TiO₂ failed to retain the reversible capacity upon cycling, keeping only 23% of the initial value after 80 cycles. X-ray photoelectron spectroscopy (XPS) results together with electrochemical data suggest that the failure in cyclability is of kinetic nature as the loss in specific charge is not completely irreversible. Thermogravimetry analysis revealed that the pristine TiO₂ contained a significant amount of TiO(OH)₂ (ca. 8%) which can be easily removed by dehydration when annealing in air above 250 °C. Air-annealing of TiO₂ at 300 °C resulted in a remarkable improvement in cyclability retaining 83% of initial specific charge after 80 cycles at 0.5C. No further improvement in cyclability was observed for TiO₂ annealed at 450 °C suggesting that the dehydration of TiO(OH)₂ was the primary source of the improvement. Knowing the role of dehydration of TiO₂ allows obtaining a reliable benchmark material via simple air-annealing and becomes a key factor when developing advanced materials from commercial TiO₂.

© 2014 Elsevier B.V. All rights reserved.

1. Introduction

Energy storage plays a key role in achieving a sustainable energy system. Among different existing technologies, Li-ion batteries (LIBs) are receiving much attention mainly due to their high specific energy density [1–3]. For negative electrodes, titania-based materials offer additional safety, especially at temperatures above 60 °C, longer cycle stability and a safe potential gap to lithium electroplating for high-power applications [4], which may compensate in some cases for their lower energy density. Indeed, batteries

employing Li₄Ti₅O₁₂ as negative electrode material have been commercialized [5,6]. TiO₂ has been hence explored as alternative negative electrode material due to its mature synthesis methods and its higher theoretical Li-ion storage capacity of 335 mAh g^{−1} versus 175 mAh g^{−1} for Li₄Ti₅O₁₂. However, the practical specific charge of TiO₂, which is typically around 160 mAh g^{−1}, is still far from the theoretical one and unlocking the potential of TiO₂ remains a challenge.

There are two main limitations that prevent TiO₂ from achieving higher practical specific charge values: 1) the poor electric conductivity and 2) the slow Li-ion diffusivity. The conductivity has been successfully improved by e.g. wiring with carbon nanotubes [7], carbon [8] and RuO₂ [9] coatings or introducing different types of doping agents [10]. The slow diffusivity has been addressed by

* Corresponding author. Tel.: +49 234 3228202; fax: +49 234 3214683.

E-mail address: edgar.ventosa@rub.de (E. Ventosa).

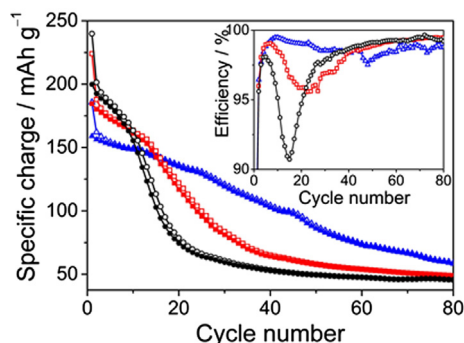


Fig. 1. Specific charge of the as-received TiO_2 samples cycled within three different potential windows: 3–1.0 V (circles), 3–1.2 V (squares) and 3–1.5 V (triangles), at 0.5C rate. Discharge and charge are assigned with open and closed symbols, respectively. Inset: Coulombic efficiency on cycling in the corresponding three different potential windows.

e.g. nanostructuring [11], mesoporosity [12] or tuning the crystal phase [13].

TiO_2 is often proposed for high power applications because its operating potential is more than 1 V above lithium electroplating. Therefore, the majority of studies involving the use of TiO_2 for LIBs investigate the specific charge retention at high C-rates. However, it has been shown in several studies that TiO_2 anatase nanoparticles have poor cyclability [7,10,14–16]. A possible cause of specific charge fading proposed by Shin et al. [15] is related to the slow bulk intercalation. The Li-ion extraction from the bulk is strongly hindered leading to losses in activity of the bulk. Nevertheless, no

systematic study has been performed to understand the origin of the decrease in specific charge that is crucial to enable the use of commercial TiO_2 as a platform for further improvement.

Here, we investigated the source of poor cyclability observed in commercial TiO_2 anatase nanoparticles by means of electrochemistry, X-ray photoelectron spectroscopy (XPS), Raman spectroscopy, infrared spectroscopy and thermogravimetry analysis. Understanding of the failure allowed us to largely improve the cyclability by subjecting the pristine material to a simple air-annealing process. The resulting material can be employed as reliable benchmark material when TiO_2 is modified, e.g. carbon coating, doping, etc, or TiO_2 with particular features, e.g. shape or phase, or special synthesis is obtained.

2. Experimental

Anatase TiO_2 nanoparticles with a specific surface area of ca. $100 \text{ m}^2 \text{ g}^{-1}$ (ca. 15–20 nm particle size) and provided by Sachtleben Chemie were used as received unless specified otherwise. The pristine TiO_2 sample was annealed at 300 or 450 °C in synthetic air for 1 h. The obtained samples are referred to as $\text{TiO}_2@300$ or $\text{TiO}_2@450$, respectively. Electrode slurries were prepared with 76:15:9 wt% composition of active material, C65 carbon black (Timcal) and polyvinylidene difluoride (PVdF) binder solution (Solef S5130, Solvay) dispersed in *N*-methyl pyrrolidone (NMP) (Sigma–Aldrich) and mixed thoroughly for 30 min at 4000 rpm using an ultra-turrax disperser (Ika). The slurry was then deposited onto a copper current collector (15 μm) using the “doctor blade” technique (200 μm film thickness) and dried at 60 °C for 2 h. 12 mm disk electrodes were punched out with a commercially available

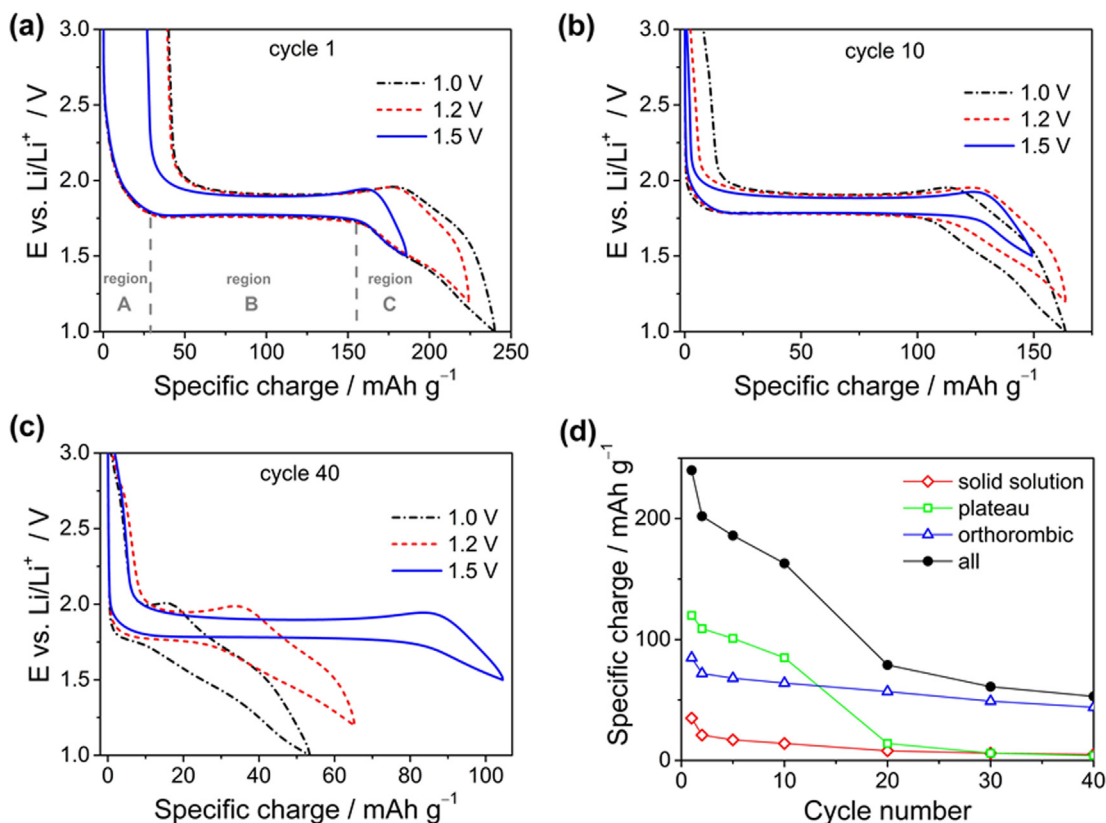


Fig. 2. (a)–(c) Discharge profile of the as-received TiO_2 samples cycled within three different potential windows at 0.5C rate, for the cycles: 1, 10 and 40. (d) Representation of the specific charge corresponding to different regions of the discharge profile of the as-received TiO_2 sample cycled within 3–1 V potential window at 0.5C rate.

hole punch (Hoffmann) and dried overnight at 110 °C in a vacuum oven (Büchi) resulting in an active material loading of ca. 2 mg cm⁻². Cells were assembled in an argon-filled glove box (O₂ < 2 ppm and H₂O < 1 ppm). Metallic lithium (Sigma–Aldrich, *d* = 0.38 mm) was used as counter and reference electrodes, Whatman GF/D glass fibre filter as separator and 1 M LiPF₆ in ethylene carbonate (EC):diethyl carbonate (DEC), 1:1 wt% (LP40, Merck) as electrolyte.

Galvanostatic cycling (GC) experiments were carried out using a Bio-Logic VMP-3 potentiostat (Bio-Logic). Charge/discharge rates of 0.5C (assuming the theoretical capacity of TiO₂ as 330 mA g⁻¹) were applied during cell cycling within different potential windows: 3.0 V–1.0 V, 3.0 V–1.2 V and 3.0 V–1.5 V. All potentials are reported versus Li/Li⁺ and all electrochemical experiments were performed with a 3-electrode cell setup using standard Swagelok® T-cells.

XPS measurements were carried out in an UHV set-up equipped with a GammaData-Scienta SES 2002 analyser. The base pressure in the measurement chamber was 5 × 10⁻¹⁰ mbar. Monochromatic Al K_α (1486.6 eV; 14.5 kV; 30 mA) was used as incident radiation and a pass energy of 200 eV was chosen resulting in an energy resolution better than 0.6 eV. Charging effects were compensated using a flood gun, and binding energies were calibrated based on positioning the main C 1s peak at 284.5 eV which originates from carbon black.

TG-MS analysis was carried out in a Cahn TG2131 thermobalance coupled with a quadrupole mass spectrometer (Balzers Instrument, OmniStar). Samples were heated to 850 °C with a heating rate of 5 K min⁻¹ in synthetic air with a total flow rate of 30 sccm.

Raman measurements were performed with a Nexus FT-NIR spectrometer equipped with a nitrogen-cooled germanium detector and a 1064 nm laser (Nd:YAG) provided by Thermo Fisher Scientific. Comparability was achieved using similar amounts of sample and identical measurement parameters.

Infrared spectra of the powder samples were measured in diffuse reflectance using a Thermo Nicolet Protégé 460 spectrometer. The samples were diluted with KBr (sample-to-KBr ratio = 1:100), thoroughly ground in a mortar and placed inside a Harrick HVC-DRP-2 in situ cell with a Praying Mantis mirror construction. The samples were measured against a KBr background after purging in inert gas to remove gas-phase water.

3. Results and discussion

3.1. Effect of potential window during cycling

Adjusting the potential window for the electrochemical cycling strongly influences the performance of titania electrodes by preventing parasitic side reactions, as proposed in earlier reports [17,18]. As-received commercial anatase TiO₂ nanoparticles delivered a poor cyclability showing a rapid decay in reversible specific charge during the first few cycles in the electrochemical window of 3.0–1.0 V as shown in Fig. 1. The lower cut-off potential (COP) was raised from 1.0 V to 1.2 V and 1.5 V, respectively, in an attempt to improve the cyclability by avoiding any possible solid electrolyte interphase (SEI) formation and by reducing the strain within the particles [19]. Raising the lower COP delayed the fading in specific charge (Fig. 1) and it increased the efficiency (inset in Fig. 1). However, it was not possible to prevent the failure in cyclability by controlling the potential window and similar capacity values were obtained for all potential windows after 80 cycles.

To gain insight into the mechanism of the specific charge fading, we evaluated the losses in the different storage domains of TiO₂. Fig. 2a–c shows the potential profiles of intercalation/de-intercalation of as-received TiO₂ at three COPs for the 1st, 10th and 40th cycle, respectively. According to Wagemaker et al. [20], each intercalation and de-intercalation profile can be divided into

three regions. Region A or solid solution domain occurs above 1.8 V and Li-ions are inserted into or extracted from the tetragonal phase without phase transformation. The charge capacity of Li-ion storage is low and it takes place only near the surface. Region B or phase transformation domain, tetragonal–orthorhombic, is giving rise to a potential plateau at ca. 1.8 V. During the phase transformation up to 0.5 Li per Ti can be inserted corresponding to 168 mAh g⁻¹. Region C or orthorhombic phase domain occurs below ca. 1.8 V and corresponds to compositions varying from Li_{0.5}TiO₂–Li₁TiO₂. The mechanism of insertion/extraction in region C is under debate; it was initially proposed without considering a phase transformation [15,21], but recent findings seem to support a second phase transformation in this region [20,22,23]. In any case, the Li-ion mobility in the Li-rich phase is very poor and, correspondingly, the amount of Li-ions stored in this domain is heavily depending on the particle size and the specific surface area. The larger the surface area is, the shorter the Li-ion pathway inside the particle and the higher the specific charge achieved. Fig. 2a shows that the specific charge of the examined samples decreased with increasing COP due to the decreased amount of Li-ion stored in region C. The capacities for the three COPs reached similar values after 10 cycles (Fig. 2b). Actually, the specific charge at the 10th cycle for the COP of 1.5 V was slightly lower than those of 1.2 V and 1.0 V, however, the length of the phase transformation plateau for 1.5 V was larger than those for 1.2 V and 1.0 V COPs. It seems that the decay in specific charge originated from shortening of the phase transformation plateau. Potential profiles at cycle 40, Fig. 2c, clearly confirmed this plateau shortening. As a matter of fact, the specific charge for the COP of 1.0 V exclusively derived here from region C while region B hardly contributed. In order to easily visualize the contribution of each region to the failure in cyclability, we plotted the evolution of the specific charge of each region with cycles as well as the evolution of the overall specific charge for the COP of 1.0 V (Fig. 2d). After an initial general decay in all regions, most likely due to the irreversible specific charge losses, the evolution of the overall specific charge profile follows that of the phase transformation domain (region B). Thus, the decay in the reversible specific charge is mostly due to the loss in the phase transformation region. It is not clear why TiO₂ loses the ability to undergo phase transformation upon cycling. Structural degradation of TiO₂ or entrapment of Li-ions that occupy the sites of the tetragonal phase may prevent the tetragonal–orthorhombic transformation.

3.2. Kinetic origin of reversible specific charge storage losses

We explored the nature of the losses in reversible specific charge to determine whether de-intercalation was kinetically limited or thermodynamically impeded. For that purpose, we investigated the effect of holding the potential at 3.0 V for a long time at the end of a cycle. As-received TiO₂ was aged between 3.0 V and 1.0 V for 80 cycles. After the sample reached again 3.0 V, a potentiostatic step was applied for 10 h (only after the 80th cycle). If the losses in specific charge occurring over the 80 cycles were irreversible, the charge flow should be negligible during the potentiostatic step. However, an additional specific oxidation charge of 141 mAh g⁻¹ was flowing during the potentiostatic step after the 80th cycle. It should be noted that the difference between the specific reduction charge in the 81st cycle and in the 80th cycle was equal to 122 mAh g⁻¹, as shown in Fig. 3a, thus being in good agreement with the additional specific oxidation charge. This additional specific oxidation charge can originate from kinetically hindered de-intercalation of Li-ions from the titania and/or oxidation of the SEI. We employed XPS to distinguish between these two possibilities. XPS spectra of as-received TiO₂ were obtained i) before cycling, ii) at the end of the

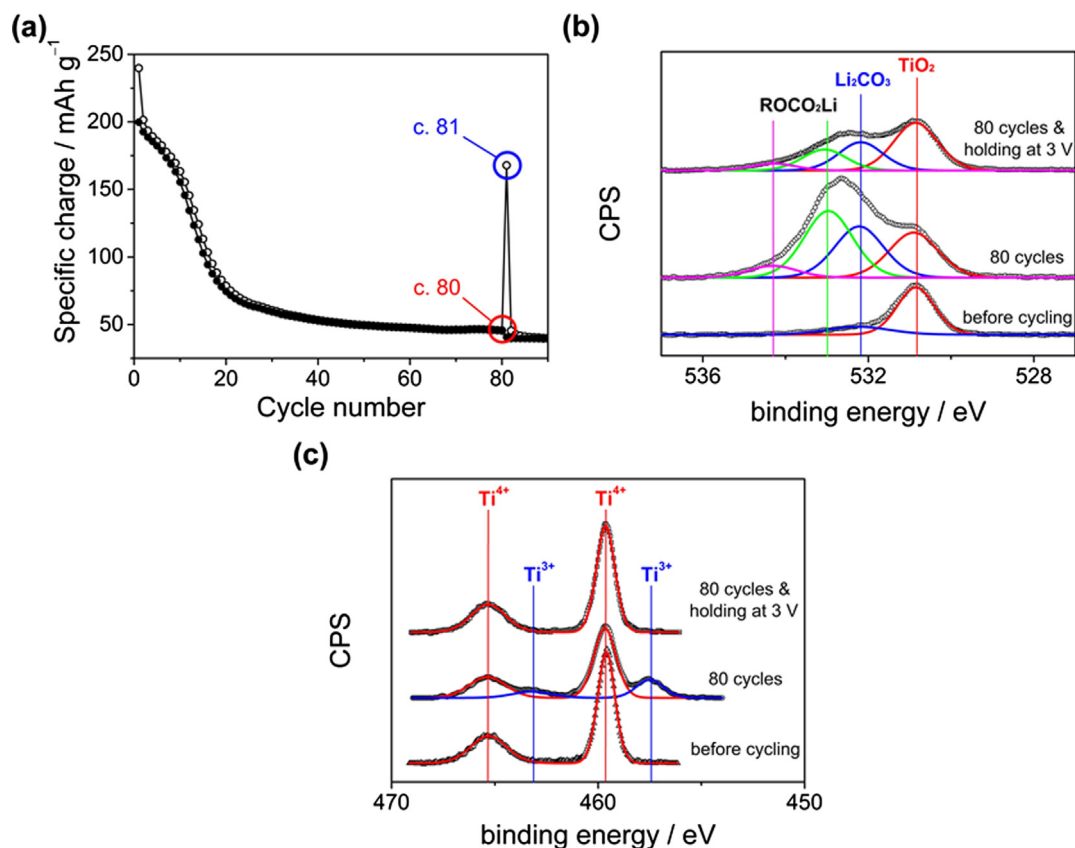


Fig. 3. (a) Specific charge profile of the as-received TiO₂ sample cycled within the 3–1 V potential window at 0.5C rate. Prior to the 81st intercalation, the potential was held at 3 V for 10 h; XPS spectra of the as-received TiO₂ samples for the (b) O 1s and (c) Ti 2p regions taken before cycling, at the end of the 80th cycle and at the end of 80th cycle followed by holding the potential at 3.0 V for 10 h, cycled within the 3–1 V potential window at 0.5C.

80th cycle without potentiostatic step, and iii) at the end of the 80th cycle with potentiostatic step (Fig. 3b and c). We evaluated O 1s and Ti 2p spectral regions. Information about the oxidation of the SEI can be extracted from the O 1s region (Fig. 3b), as reported previously [24]. The intensity of the signal was normalized to the metal oxide signal for better comparison as the SEI covers the surface of TiO₂ weakening the signal of the metal oxide. Before cycling, the spectrum shows a weak signal of lithium carbonate originating from the electrolyte. After 80 cycles, XPS revealed a larger amount of lithium carbonate and the presence of several types of lithium alkyl carbonates. The overall signal of carbonates with respect to the metal oxide is much stronger after cycling. Holding the potential at 3.0 V led to the weakening of the organic carbonate peaks, which indicates a partial oxidation and a thinning-out of the SEI film, similar as shown in the case of graphite electrodes [25]. Moreover, the ratio between the signals of the different carbonates changed, which supports a transformation in the SEI composition. On the other hand, the Ti 2p region revealed that ca. 25% of titanium remains as Ti³⁺ at the end of the 80th cycle when the potentiostatic step is not applied, which means that some Li-ions are still trapped inside the particles (Fig. 3c). Holding the potential at the end of the 80th cycle successfully re-oxidizes all Ti³⁺ ions back to Ti⁴⁺, releasing the entrapped Li-ions. This oxidation of Ti³⁺ ions results in an amount of anodic specific charge that equals to ca. 85 mAh g⁻¹. Thus, the entrapment of Li-ions and the oxidation of the SEI contribute with ca. 85 mAh g⁻¹ and ca. 56 mAh g⁻¹, respectively, to the additional specific oxidation charge flowing during the potentiostatic step.

3.3. Origin and mitigation of kinetically limited Li-ion storage

The failure in cyclability is not completely irreversible, as indicated by electrochemical and XPS results, where insertion and extraction of Li-ions become kinetically hindered leading to the entrapment of Li-ions inside the particles. Understanding the origin of this behaviour is crucial to potentially overcome the failure. Low crystallinity or remaining residues from the synthesis that lead to side electrochemical reactions are among the possible sources triggering the hindered Li-ion mobility. Both unfavourable conditions should be largely removed by annealing of the commercial TiO₂ resulting in improved cyclability. Thermogravimetry analysis (TG) was performed using as-received commercial TiO₂ (Fig. 4a). A significant mass loss of 3% was found when annealing in synthetic air to up to 850 °C. The differential of the TG curve assists in identifying the temperatures at which the main losses of mass occur. There were two strong peaks in the differential curve at 100 °C and 220 °C and two weak peaks at 475 °C and 800 °C. The loss of mass taking place at around 100 °C is assigned to the release of water adsorbed at the surface of TiO₂ and it accounts for almost 1% (30 °C–160 °C). The second region with a peak located at 220 °C is likely associated with dehydration of remaining TiO(OH)₂ and the loss of mass centred around that temperature (160 °C–300 °C) was 1.5%. The release of 1.5% of water would mean that TiO(OH)₂ accounts for 8.2% of the initial mass, which is a significant amount. The two last regions may be related to the decomposition of some remaining residues from the synthesis. Mass losses of 0.25% and 0.1% were observed around the third peak located at 475 °C (400 °C–600 °C) and the fourth peak at 800 °C (600 °C–850 °C),

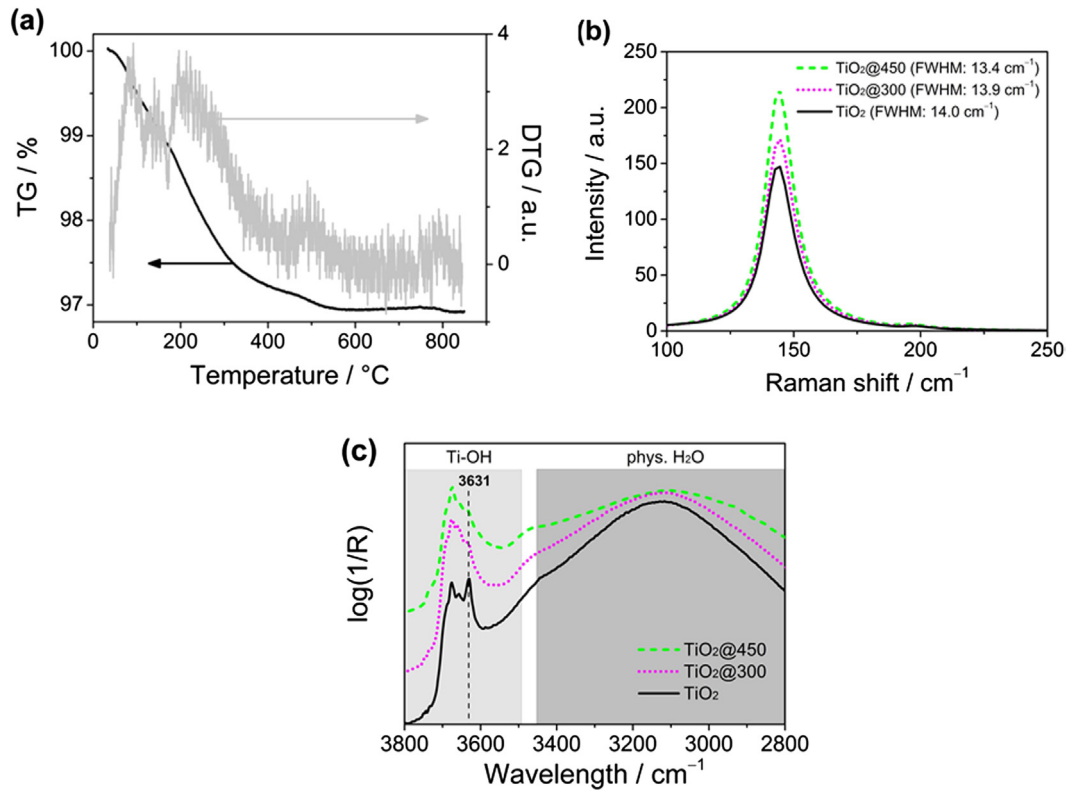


Fig. 4. (a) TG analysis during annealing in synthetic air up to 850 °C of the as-received commercial TiO₂ sample and the differential of the TG curve (DTG); (b) Raman and (c) infrared (DRIFTS) spectra of the as-received TiO₂ sample and after annealing at 450 °C and 300 °C in air for 1 h.

respectively. The thermobalance was coupled with mass spectroscopy (TG-MS) recording the evolution of 18, 28, 30, 44 and 48 mass to charge ratios. However, TG-MS did not provide additional information about the annealing process since only the release of water was detected. Water adsorbed at the surface is released anyway during the electrode preparation by drying at 110 °C under vacuum for 12 h. Thus, we decided to anneal the as-received TiO₂ either at 300 °C or at 450 °C. The former will only lead to the dehydration of the remaining TiO(OH)₂, while the latter will cause both dehydration of the TiO(OH)₂, as well as an increase in the crystallinity of the anatase phase and decomposition of some remaining residues.

Pristine TiO₂, TiO₂@300 and TiO₂@450 were investigated by Raman spectroscopy to evaluate their crystalline phase (Fig. 4b). Raman spectra confirmed anatase being the only phase in the three samples. Changes in the degree of crystallinity and the crystalline particle size can be estimated from Raman spectroscopy results. According to Zhang et al. [26], the frequency and the line width of the E_g Raman mode of the anatase phase is suitable to estimate the crystals particle size. Within the error of the measurement, the Raman frequency of the peak maximum did not change and the width of the peaks becomes only slightly narrower. Thus, no significant change in crystallinity or particle size can be observed upon annealing at 300 °C or 450 °C.

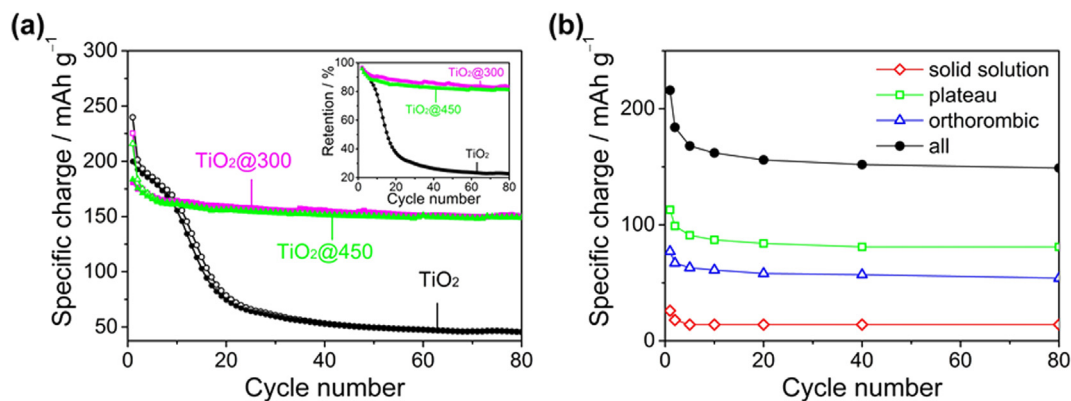


Fig. 5. (a) Specific charge profile and retention profile (inset in a) for the as-received TiO₂ and annealed samples at 450 °C and 300 °C in air for 1 h, cycled within the 3–1 V potential window at 0.5C rate. Discharge and charge capacities are assigned with open and closed symbols, respectively. (b) Representation of the specific charge corresponding to different regions of the discharge profile of the TiO₂ sample annealed at 450 °C in air for 1 h, cycled within the 3–1 V potential window at 0.5C rate.

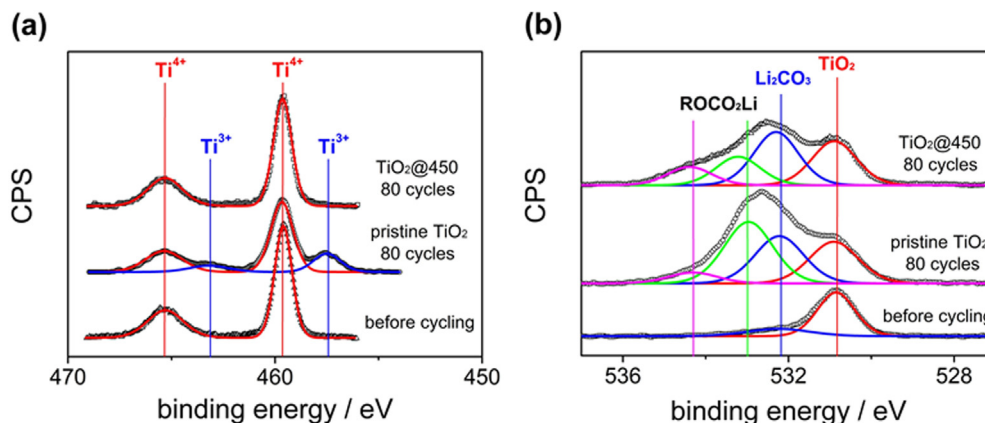


Fig. 6. XPS spectra for the (a) Ti 2p and (b) O 1s regions of the TiO_2 sample annealed at 450°C in air for 1 h, taken before and after aging for 80 cycles within the 3–1 V potential window at 0.5C rate.

Diffuse reflectance infrared spectroscopy (DRIFTS) was performed to characterize the OH groups on the surfaces of pristine TiO_2 , $\text{TiO}_2@300$ and $\text{TiO}_2@450$ materials and to gain further insights into feasible removal of surface residues [27]. As shown in Fig. 4c, the ratio between the different OH groups on the surface of the TiO_2 material drastically changed upon calcination at 300°C and 450°C . Furthermore, it is evident that less water is physisorbed on the surface of the materials upon calcination. Thus, it is likely that specific surface sites favouring water adsorption are removed upon calcination.

The cyclability of air-annealed TiO_2 electrodes was evaluated by aging the electrodes for 80 cycles at 0.5C (Fig. 5a). As explained in the previous section, as-received TiO_2 was able to retain only 23% of the initial reversible specific charge after 80 cycles. In contrast, both $\text{TiO}_2@300$ and $\text{TiO}_2@450$ showed improved capacity retention of 83% and 81% after 80 cycles, respectively (inset in Fig. 5a). The losses in reversible specific charge for $\text{TiO}_2@300$ and $\text{TiO}_2@450$ did not originate in the phase transformation domain as observed for as-received TiO_2 , but they derived equally from the three regions (Fig. 5b). According to the TG results, the remarkable improvement achieved by annealing at 300°C is due to the dehydration of ca. 1.5% of $\text{TiO}(\text{OH})_2$. Annealing at 450°C did not improve the cyclability obtained for 300°C . Therefore, the presence of $\text{TiO}(\text{OH})_2$ remaining from the synthesis is critical for the cyclability of TiO_2 as negative electrode material in Li-ion batteries.

We employed XPS again to evaluate the presence of Ti^{3+} and the SEI in the air-annealed sample $\text{TiO}_2@450$ after 80 cycles. Ti^{3+} was not detected in $\text{TiO}_2@450$ (Fig. 6a), indicating that the annealing process prevents the entrapment of Li-ions upon cycling. On the other hand, the SEI was also observed for $\text{TiO}_2@450$ (Fig. 6b), although it was thinner (as indicated by the weaker carbonate signal) and had a different composition, that is different ratio of lithium alkyl carbonates species than that for as-received TiO_2 . XPS results assist in understanding the trend observed for the potential separation of de-intercalation.

4. Conclusions

The failure in cyclability of commercially available TiO_2 as negative electrode material in Li-ion batteries with retention of only 23% of the initial specific charge after 80 cycles cannot be overcome by limiting the operating electrochemical window. From the three Li-ion intercalation domains of TiO_2 , the tetragonal–orthorhombic transformation domain suffers the most in terms of reversible specific charge losses. The failure in cyclability is of

kinetic nature as the losses are not completely irreversible. The intercalation/de-intercalation process becomes kinetically hindered upon cycling and entrapped Li-ions remain in TiO_2 at the end of the cycle. The pristine commercial TiO_2 used in this study contains a significant amount of $\text{TiO}(\text{OH})_2$, ca. 8%, which can be easily removed by dehydration in air above 250°C . The cyclability was largely improved by annealing in air at 300°C for 1 h leading to reversible specific charge retention of 83% after 80 cycles at 0.5C. Annealing at higher temperatures such as 450°C did not further improve the electrochemical performance of TiO_2 -based negative electrodes. Therefore, the dehydration of $\text{TiO}(\text{OH})_2$ remaining from the synthesis is identified as the main source of improvement, rather than enhancing the crystallinity of the material or removing surface impurities. The strong influence of OH groups on the SEI properties, e.g. thickness and composition, may trigger the entrapment of Li-ions and the general failure in cyclability of as-received TiO_2 . Consequently, air-annealing becomes a requirement when using commercial TiO_2 as a negative electrode in Li-ion batteries. Although, the process might not be necessary for particular commercial TiO_2 materials containing very low amounts of $\text{TiO}(\text{OH})_2$.

Acknowledgements

The financial support by the Federal Ministry of Education and Research (BMBF) in the framework of the project “BatMat” (FKZ 13N11399), the funding of the Centre for Electrochemical Sciences (CES) by the European Commission and the state North Rhine-Westphalia (NRW) in the framework of the HighTech. NRW program are gratefully acknowledged. We thank Dr. Jennifer Struck for her help in infrared spectroscopy.

References

- [1] M.S. Whittingham, *Chem. Rev.* 104 (2004) 4271.
- [2] A.S. Arico, P. Bruce, B. Scrosati, J.-M. Tarascon, W. van Schalkwijk, *Nat. Mater.* 4 (2005) 366.
- [3] J.-M. Tarascon, M. Armand, *Nature* 414 (2001) 359.
- [4] Z. Chen, I. Belharouak, Y.-K. Sun, K. Amine, *Adv. Funct. Mater.* 23 (2013) 959.
- [5] A. Du Pasquier, C. Huang, T. Spetler, *J. Power Sources* 186 (2009) 508.
- [6] T. Tan, H. Yumoto, D. Buck, B. Fattig, C. Hartzog, *World Electr. Veh. J.* 2 (2008) 76.
- [7] E. Ventosa, P. Chen, W. Schuhmann, W. Xia, *Electrochem. Commun.* 25 (2012) 132.
- [8] F.-F. Cao, X.-L. Wu, S. Xin, Y.-G. Guo, L.-J. Wan, *J. Phys. Chem. C* 114 (2010) 10308.
- [9] Y.-G. Guo, Y.-S. Hu, W. Sigle, J. Maier, *Adv. Mater.* 19 (2007) 2087.

- [10] E. Ventosa, W. Xia, S. Klink, F. La Mantia, B. Mei, M. Muhler, W. Schuhmann, *Chem. Eur. J.* 19 (2013) 14194.
- [11] C. Jiang, M. Wei, Z. Qi, T. Kudo, I. Honma, H. Zhou, *J. Power Sources* 166 (2007) 239.
- [12] K. Saravanan, K. Ananthanarayanan, P. Balaya, *Energy Environ. Sci.* 3 (2010) 939.
- [13] E. Ventosa, B. Mei, W. Xia, M. Muhler, W. Schuhmann, *ChemSusChem* 6 (2013) 1312.
- [14] G. Sudant, E. Baudrin, D. Larcher, J.-M. Tarascon, *J. Mater. Chem.* 15 (2005) 1263.
- [15] J.-Y. Shin, D. Samuelis, J. Maier, *Adv. Funct. Mater.* 21 (2011) 3464.
- [16] J.-Y. Shin, J.H. Joo, D. Samuelis, J. Maier, *Chem. Mater.* 24 (2012) 543.
- [17] P. Kubiak, J. Geserick, N. Hüsing, M. Wohlfahrt-Mehrens, *J. Power Sources* 175 (2008) 510.
- [18] P. Kubiak, T. Fröschl, N. Hüsing, U. Hörmann, U. Kaiser, R. Schiller, C.K. Weiss, K. Landfester, M. Wohlfahrt-Mehrens, *Small* 7 (2011) 1690.
- [19] G. Zampardi, E. Ventosa, F. La Mantia, W. Schuhmann, *Chem. Commun.* 49 (2013) 9347.
- [20] M. Wagemaker, W.J.H. Borghols, F.M. Mulder, *J. Am. Chem. Soc.* 129 (2007) 4323.
- [21] Y. Ren, L.J. Hardwick, P.G. Bruce, *Angew. Chem.* 49 (2010) 2570.
- [22] U. Lafont, D. Carta, G. Mountjoy, A.V. Chadwick, E.M. Kelder, *J. Phys. Chem. C* 114 (2010) 1372.
- [23] V. Gentili, S. Brutti, L. Hardwick, A. Armstrong, S. Panero, P. Bruce, *Chem. Mater.* 24 (2012) 4468.
- [24] S. Brutti, V. Gentili, H. Menard, B. Scrosati, P.G. Bruce, *Adv. Energy Mater.* 2 (2012) 322.
- [25] H. Bryngelsson, M. Stjerndahl, T. Gustafsson, K. Edstrom, *J. Power Sources* 174 (2007) 970.
- [26] W.F. Zhang, Y.L. He, M.S. Zhang, Z. Yin, Q. Chen, *J. Phys. D Appl. Phys.* 33 (2000) 912.
- [27] L. Liu, H. Zhao, J.M. Andino, Y. Li, *ACS Catal.* 2 (2012) 1817.